Development 122, 3217-3228(1996)
Printed in Great Britain © The Company of Biologists Limited 1996
DEV4751

Mice with targeted disruption of *Hoxb-1* fail to form the motor nucleus of the VIIth nerve

Judy M. Goddard, Mireille Rossel, Nancy R. Manley and Mario R. Capecchi*

Howard Hughes Medical Institute, Department of Human Genetics, University of Utah, School of Medicine, Salt Lake City, Utah 84112, USA

*Author for correspondence

SUMMARY

Mice were generated with targeted disruptions in the *hoxb-1* gene. Two separate mutations were created: the first disrupts only the homeodomain and the second inactivates the first exon as well as the homeodomain. The phenotypes associated with these two mutant alleles are indistinguishable in surviving adult mice. The predominant defect in these mutant mice is a failure to form the somatic motor component of the VIIth (facial) nerve, possibly through a failure to specify these neurons. The phenotype of *hoxb-1* mutant homozygotes closely resembles features of the clinical profile associated with humans suffering from Bell's Palsy or Moebius Syndrome. These animals should therefore provide a useful animal model for these human diseases.

Key words: Hox genes, homeobox genes, *hoxb-1*, facial nerve, Bell's Palsy, Moebius Syndrome, mouse development, gene targeting

INTRODUCTION

Mice and humans contain at least 39 *Hox* genes distributed on four linkage groups, designated Hox A, B, C and D, on four separate chromosomes. Based on DNA sequence similarities and on the positions of the genes on their respective chromosomes, individual members of the four linkage groups have been classified into 13 paralogous families. These genes encode transcription factors belonging to the *Antennapedia* homeodomain class. The homologous genes in *Drosophila* are used to pattern the developing embryo (Lewis, 1978). Mutational analysis in the mouse has demonstrated that these genes, alone or in concert with other *Hox* genes, are used to regionalize the embryo along its major axes (Chisaka and Capecchi, 1991; Lufkin et al., 1991; Chisaka et al., 1992; LeMouellic et al., 1992; Dollé et al., 1993; Gendron-Maguire et al., 1993; Jeannotte et al., 1993; Ramirez-Solis et al., 1993; Rijli et al., 1993; Small and Potter, 1993; Davis and Capecchi, 1994; Kostic and Capecchi, 1994; Davis et al., 1995; Horan et al., 1995; Manley and Capecchi, 1995; Rancourt et al., 1995; Satokata et al., 1995; Suemori et al., 1995; Boulet and Capecchi, 1996; Davis and Capecchi, 1996; Favier et al., 1996; Fromental-Ramain et al., 1996). Thus, mutations in 3′ *Hox* genes affect the formation of anterior embryonic structures, whereas disruption of 5′ genes gives rise to posterior abnormalities. In addition to being used to regionalize the embryo along the major axes, *Hox* genes also appear to be used to regionalize subcomponents of the embryo such as the gut, the reproductive organs and the limbs (Yokouchi et al., 1991, 1995; Roberts et al., 1995; Dollé et al., 1989, 1991; Izpisúa-Belmonte et al., 1991). Regionalization of the embryo by *Hox* genes appears to be accomplished by the controlled temporal and spatial activation of these genes such that a 3′ gene is activated prior to and in a more anterior region of the embryo than its 5′ neighbor (Duboule and Dollé, 1989; Graham et al., 1989). This cascade of gene activation generates a nested set of *Hox* gene transcripts along the embryonic axes and in the embryonic subcomponents. As a result, each region is characterized by expression of a specific complement of *Hox* genes. The complement of *Hox* genes in turn activates a region-specific developmental program and thereby orchestrates the morphological regionalization of the embryo. Indeed, through their ordered position on the chromosomes, a fundamental property of *Hox* genes may be their ability to convert a series of temporally ordered transcriptional events into a directed, ordered series of morphological events.

In this report, we examine the effects on mouse development of disrupting the *hoxb-1* gene, the most 3′ member of the Hox B linkage group. After 8.5 days of gestation (E8.5), rostral expression of *hoxb-1* is limited in the hindbrain to rhombomere 4 and to the neural crest cells migrating from this rhombomere. *Hoxb-1* mutant mice do not have any apparent defects in tissues derived from this neural crest cell population. However, formation of the somatic motor component of the facial nerve is severely compromised in these mutants. Defects are also seen in the facial musculature. Both of these defects may be tied to a failure to specify the population of motor neurons that is normally generated in rhombomere 4 and destined to contribute to the facial motor nucleus in the hindbrain.

MATERIALS AND METHODS

Targeting vector

Genomic DNA surrounding and including the *hoxb-1* locus was isolated

from a 129Sv mouse library in lambda FIX II (Stratagene). Exon I was inactivated by insertion of a 12 bp *Bam*HI linker into the unique *Eag*I site. The homeodomain in exon II was disrupted by replacement of a 371 bp *Bgl*II fragment in this exon (Frohman et al., 1990) with the neomycin resistance (*neo*^{r}) gene from MC1neopA (Thomas and Capecchi, 1987). The mutated sequences included in 12 kb of genomic DNA were cloned into a pUC-based vector containing the herpes simplex virus *thymidine kinase* genes, *TK1* and *TK2* (Fig. 1A).

Generation of *hoxb-1* mutant mice

The targeting vector described above was linearized and electroporated into R1 ES cells (Nagy et al., 1993). Following positive/negative selection in G418 and FIAU (Mansour et al., 1988), Southern blot analysis was used to identify the homologous recombinants (Fig. 1 and below). The accuracy of the recombination events was verified by a variety of restriction enzyme digests and three different probes. The latter included the 5′-flanking probe, a probe specific for the *neo*^{r} gene, and a 750 bp internal probe extending from the *Eag*I site in exon I to an *Xba*I site in the intron. Positive cell lines were injected into blastocysts. The resulting male chimeric mice were bred with C57BL/6J (BL/6) females, and offspring carrying the mutation in the germ line were identified by Southern blot analysis (Fig. 1B and below).

Genotype analysis

Adult mice were genotyped by Southern blot analysis or by gel analysis of PCR-amplified sequence from DNA purified from tail biopsies (Thomas et al., 1992). For Southern blot analysis, the DNA was digested with *Bam*HI and probed with the 5′-flanking probe. While the wild-type sequences were contained on a 6.7 kb fragment, those of *hoxb-1*^{neo} and *hoxb-1*^{neoB} were detected as 7.7 kb and 5.2 kb fragments, respectively (Fig. 1B).

The primers used for PCR amplification were as follows: *Hoxb-1* sense primer, 5′AAGGTGTCCGAGCTGGGACTG (nucleotides 663-684, Frohman et al., 1990); *hoxb-1* antisense primer, 5′CCAGCCATCAATCATCCCTCCA (nucleotides 1182-1161, Frohman et al., 1990); *neo* sense primer, 5′GCCTGCTTGCCGAATATCATGG (225 bp from the 3′-end of the *neo* gene, Beck et al., 1982). PCR cycling times were 94°C, 30 seconds; 61°C, 30 seconds; 72°C, 30 seconds for 30 cycles with a 1 second/cycle extension at 72°C. Amplified products were analyzed on a 1.5% TreviGel 500 (Trevigen). The wild-type band was 520 bp; that of the *neo* allele was 373 bp.

Yolk sacs dissected from embryos were analyzed by PCR. After incubation at 55°C overnight in PCR lysis buffer (Carpenter et al., 1993) containing proteinase K at 1 mg/ml, the samples were boiled for 5 minutes and chilled on ice; an aliquot was added to the PCR reaction mixture and analyzed as described above.

Histology

For paraffin sectioning, newborn mice were killed by CO_2 asphixiation, fixed in Bouin's and embedded in Paraplast X-Tra. 10 μm sections from 3 *hoxb-1*^{neoB} heterozygous and 3 *hoxb-1*^{neoB} homozygous animals were stained with hematoxylin and eosin, mounted in DPX and photographed as previously described (Mansour et al., 1993).

For vibratome sectioning, SWR/J embryos (E9.0 to E10.5) were fixed at 4°C overnight in 4% paraformaldehyde in phosphate-buffered saline (PBS), washed in PBS and embedded in 15% gelatin. The embedded embryos were refixed at 4°C overnight and washed with PBS before sectioning.

Immunohistochemistry

For detection of neurofilament protein, paraffin sections were dewaxed with HemoD, hydrated through a graded ethanol series and then treated for 30 minutes with 0.6% hydrogen peroxide in methanol to inactivate endogenous peroxidases. The sections were blocked in 3% goat serum in PBS (PBSG) for 60 minutes, rinsed with PBS and incubated at 4°C overnight with the 2H3 antibody directed against the 155×10^3 M_r subunit of the neurofilament protein (Dodd et al., 1988) diluted 1:1 in PBSG. Sections were washed in PBS and then incubated 2 hours with a horseradish peroxidase (HRP)-conjugated goat anti-mouse secondary antibody (Jackson Immunoresearch) diluted 1:200 in PBSG. For the HRP reaction, sections were incubated in 0.5 mg/ml diaminobenzidine (DAB) in PBS plus 0.03% hydrogen peroxide. After rinses in PBS and water, sections were counterstained in nuclear fast red, mounted in DPX and photographed as previously described (Mansour et al., 1993).

Immunostaining of hoxb-1 protein in embryos and vibratome sections of embryos was carried out with a hoxb-1 affinity-purified polyclonal antibody directed against a GST-fusion protein encoded by *hoxb-1* exon I (Manley and Capecchi, 1995). An HRP-conjugated donkey anti-rabbit secondary antibody (Jackson Immunoresearch) was used for detection of the antigen-antibody complex. The primary and secondary antibodies were used at dilutions of 1:150 and 1:400, respectively. For whole-mount staining, E9.5 embryos were fixed in 4% paraformaldehyde in PBS overnight at 4°C. Conditions for inactivation of endogenous peroxidases, incubation with the primary and secondary antibodies, and the HRP-reaction using nickel chloride were as described in Wall et al. (1992). For hoxb-1 immunostaining of vibratome sections, inactivation of endogenous peroxidases was carried out in PBS, 0.5% Triton X-100:hydrogen peroxide (4:1).

A krox-20 polyclonal antibody was generated as described by Manley and Capecchi (1995). A protein containing 87 amino acids from the beginning of the krox-20 protein (*Bcl*I-*Msc*I 257 base pair fragment, amino acids 8-95) fused to the glutathione-S-transferase gene (GST, Smith and Johnson, 1988), was made in *E. coli* and purified by adsorption to GST-sepharose beads. Purified fusion protein was injected into rabbits using a 750 mg initial lymph node injection with 750 mg intramuscular boosts. Antibodies against the krox-20 protein were affinity-purified using the krox-20-GST fusion protein after subtraction of antibodies against GST and bacterial proteins. Absence of antibodies to GST was confirmed by western blot.

Immunostaining of krox-20 protein in E8.5 (9-12 somites) embryos was performed as described above for hoxb-1 protein, except that the embryos were fixed in methanol:dimethylsulfoxide (4:1). The krox-20 primary and secondary antibodies were diluted 1:50 and 1:200, respectively.

Immunolocalization of the CRABP 1 protein was performed on E9.0 embryos as previously described (Manley and Capecchi, 1995) using a polyclonal antibody generously provided by U. Eriksson (Eriksson et al., 1987). Whole-mount embryos and vibratome sections were photographed with Ektachrome 160T film with a Wild dissecting microscope.

In situ hybridization

In situ hybridization of E9.5 embryos was performed as previously described (Manley and Capecchi, 1995). The *hoxb-2* probe was a 900 bp *Pst*I/*Hind*III fragment isolated from a cDNA clone, containing 130 bp of 3′-coding sequences and extending into the 3′-untranslated region. The probe was labelled with digoxigenin and detected with alkaline phosphatase-conjugated anti-digoxigenin Fab fragments (Jackson Immunoresearch) diluted at 1:5000.

Dye injection into cranial ganglia

Procedures used for the injection of the carbocyanine dyes, DiO and DiI (Molecular Probes), into cranial ganglia (V, VII/VIII, IX/X) have been described previously (Carpenter et al, 1993). Embryos were injected either bilaterally or unilaterally. For photography, the embryos were mounted in depression slides and viewed using fluorescein and rhodamine filter systems on a Leitz Ortholux microscope equipped with epifluorescence illumination. Animals were photographed with Kodak Ektachrome 400 film. In addition, embryos were viewed through a rhodamine filter set using a laser scanning BioRad MRC600 confocal microscope and COMOS software. Serial optical sections were combined in a superimposed 'Z series' image.

In vitro neural crest labelling

Dye injections of embryos and embryo culture were performed as previously described (Serbedzija et al., 1992; Manley and Capecchi, 1995) and analyzed by confocal microscopy.

RESULTS

Targeted disruption of the *hoxb-1* gene

Two mutant alleles of the *hoxb-1* gene, *hoxb-1*^{neo} and *hoxb-1*^{neoB}, were generated by homologous recombination between a replacement targeting vector and one of the *hoxb-1* loci in embryo-derived stem (ES) cells (Fig. 1A). The vector contained 12 kb of genomic DNA sequences flanked at the 5′ and 3′ ends by the herpes simplex virus *thymidine kinase* genes. Exon I in the vector was disrupted by insertion of a 12 bp *Bam*HI linker. This caused a frameshift mutation closely followed by termination codons in all three reading frames. Exon II of *hoxb-1* was inactivated by introduction of MC1neopA (Thomas and Capecchi, 1987) into the *Bgl*II site in helix III of the homeodomain.

The targeting vector was linearized and electroporated into R1 ES cells. Homologous recombinants were enriched by positive/negative selection (Mansour et al., 1988). Southern blot analysis of 150 selected cell lines revealed that, in five, the normal *hoxb-1* sequences had been accurately replaced with those containing MC1neopA from the vector. In four of these five, the *Bam*HI linker in exon I had also been cotransferred. The two alleles could be distinguished from each other and from the wild-type sequences by Southern transfer analysis (Fig. 1B). All positive cell lines were further analyzed with several restriction enzyme digests and internal probes to ensure that the cell lines contained no detectable rearrangements (data not shown).

Two of these cell lines, one containing only the MC1neo sequences (1g) and the other containing both the MC1neo sequences and the *Bam*HI linker in exon I (2h), were injected into blastocysts. Male chimeric mice were derived from both of these cell lines and subsequently bred to BL/6 females; analysis of the resulting progeny revealed that the mutant alleles had been transmitted through the germ line. Animals heterozygous for either mutant *hoxb-1* allele are viable and fertile.

Hoxb-1 expression in *hoxb-1* mutant alleles

The effects of the two types of mutation on the expression of hoxb-1 protein were examined in E9.5 embryos of each class subjected to whole-mount immunohistochemistry with antibody directed against amino acids encoded within exon I (Manley and Capecchi, 1995). As shown in Fig. 2, animals heterozygous for either mutant allele exhibited the expected pattern of expression in rhombomere 4 (r4), in the caudal region of the tail and in the neural crest emanating from r4. A very low level of hoxb-1 immunoreactivity was detectable in *hoxb-1*^{neo} mutant homozygous embryos, but none in the *hoxb-1*^{neoB} mutant homozygotes (Fig. 2). As shown below, the phenotypes of mice containing the two different mutant alleles are very similar; however, they are distinguishable with respect to survival.

Viability and fertility of *hoxb-1* mutant mice

Offspring generated from matings between *hoxb-1*^{neo} or *hoxb-1*^{neoB} animals were found to be present in the expected Mendelian ratios. This was true regardless of whether the crosses were performed between heterozygotes or between homozygous and heterozygous animals. Of the 20 mutant animals in the *hoxb-1*^{neo} colony allowed to mature to weaning, all but one survived. This animal died at 15 days after birth.

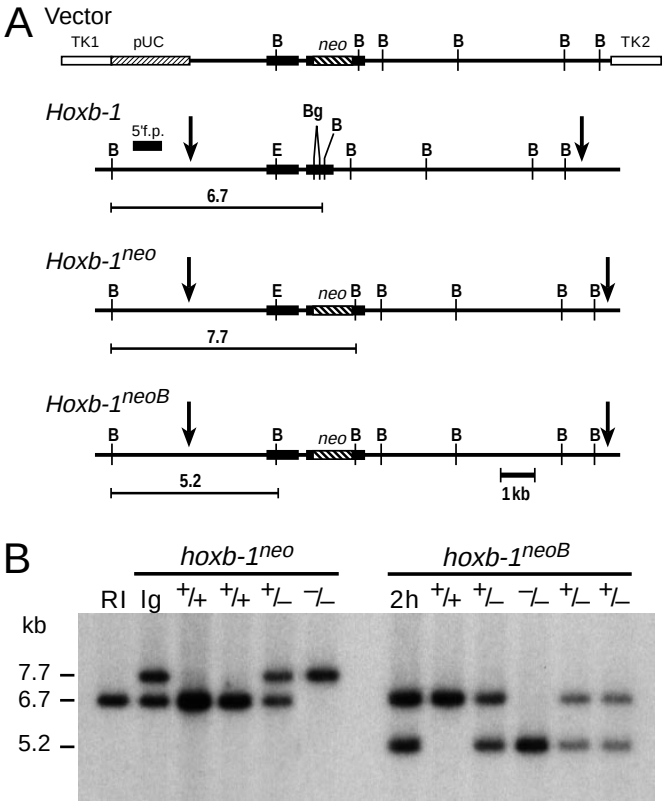

Fig. 1. Gene targeting at the *hoxb-1* locus. (A) Maps. The targeting vector (line 1) contains a 12 bp *Bam*HI linker inserted at the *Eag*I site in *hoxb-1* exon 1 and a *neo*^{r} gene that replaces a 317 bp *Bgl*II fragment within exon 2. Homologous recombination between the vector and one of the endogenous *hoxb-1* loci (line 2) in ES cells leads to two classes of G418-resistant colonies: those in which only the *neo*^{r} gene was transferred to *hoxb-1* (designated *hoxb-1*^{neo,} line 3) and those in which the *neo*^{r} gene and the *Bam*HI linker were co-transferred (designated *hoxb-1*^{neoB}, line 4). The two mutant alleles can be distinguished from each other and from the wild-type *hoxb-1* gene by Southern transfer analysis. Using the 5′ flanking probe (5′ f.p.), the wild-type gene is identified by a 6.7 kb *Bam*HI fragment whereas the *hoxb-1*^{neo} and the *hoxb-1*^{neoB} alleles will be contained on 7.7 kb and 5.2 kb fragments respectively. Thin horizontal lines represent non-coding DNA, filled boxes represent exons. Transcription of the *hoxb-1* and *neo*^{r} genes is from left to right. Vertical arrows indicate the boundaries of the genomic DNA in the targeting vector. B, *Bam*HI; Bg, *Bgl*II; E, *Eag*I. (B) Southern transfer analysis of *hoxb-1* alleles. DNA extracted from either cell lines or mouse tail biopsies was digested with *Bam*HI, and probed with the 5′ flanking probe. R1, DNA isolated from the parental (wild-type) ES cell line, R1. 1g, DNA isolated from a cell line heterozygous for the *hoxb-1*^{neo} allele. 2h, DNA isolated from a cell line heterozygous for the *hoxb-1*^{neoB} allele; +/+, +/–, –/–, DNA isolated from a representative sample of mice demonstrating the homozygous wild-type, heterozygous, and homozygous mutant genotypes of the two *hoxb-1*-mutant alleles. The sizes of the DNA fragments are indicated in kilobases.

However, 3/35 newborn *hoxb-1^{neoB}* mutant mice were found dead at birth and another 7/29 that were allowed to mature died between 15 and 24 days.

Hoxb-1 mutant mice exhibit facial paralysis

A striking characteristic of all of the adult mutant mice carrying either mutant allele is paralysis of the muscles of the face. They have little or no movement of the whiskers and nose, they do not close their eyelids in response to touch, nor do the ears move in response to touch or sound. The mutant phenotype is further evidenced by the runting of some animals, by a narrow face and by a receded lower lip, resulting in the exposure of the lower two front teeth. These lower teeth are longer and more rounded than those of control mice, suggesting reduced chewing on solid food by these animals. Although the expressivity of the whisker movement, receded lower lip and runting phenotypes was variable among mutant animals within each colony, no significant difference could be detected between the two mutant colonies. Thus, in surviving adult mice, the phenotypes of the two alleles could not be distinguished. Although the cause of death is unknown, the period with the highest death rate in the *hoxb-1^{neoB}* colony (15-24 days) corresponds to the period when the animals are changing to a solid food diet and the altered appearance

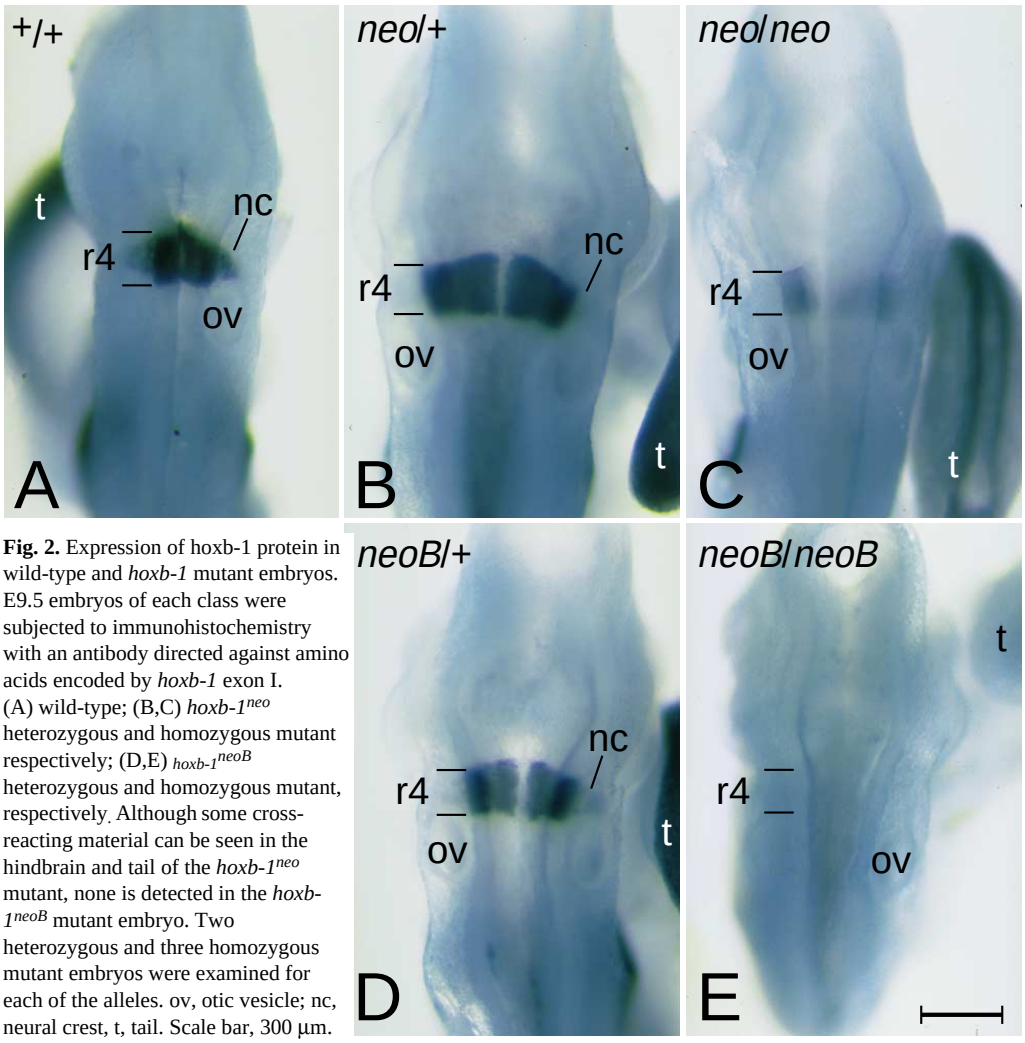

Fig. 2. Expression of hoxb-1 protein in wild-type and *hoxb-1* mutant embryos. E9.5 embryos of each class were subjected to immunohistochemistry with an antibody directed against amino acids encoded by *hoxb-1* exon I. (A) wild-type; (B,C) *hoxb-1^{neo}* heterozygous and homozygous mutant respectively; (D,E) *hoxb-1^{neoB}* heterozygous and homozygous mutant, respectively. Although some cross-reacting material can be seen in the hindbrain and tail of the *hoxb-1^{neo}* mutant, none is detected in the *hoxb-1^{neoB}* mutant embryo. Two heterozygous and three homozygous mutant embryos were examined for each of the alleles. ov, otic vesicle; nc, neural crest, t, tail. Scale bar, 300 μm.

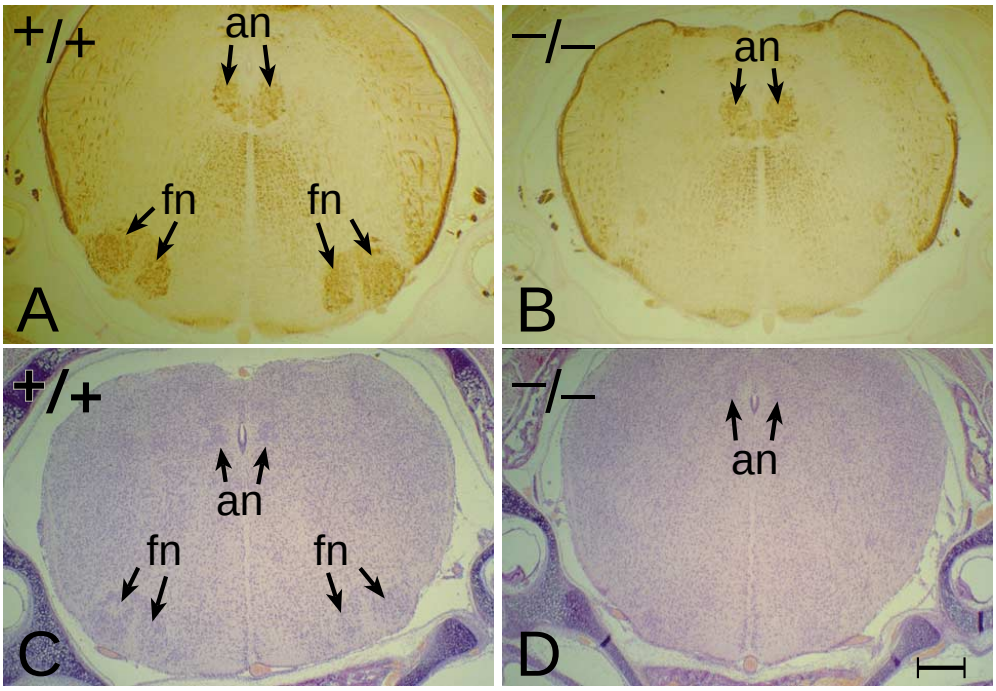

Fig. 3. Absence of the facial motor nucleus in *hoxb-1* mutant mice. Transverse, 10 μm paraffin sections of wild-type (A,C) and *hoxb-1^{neoB}* mutant (B,D) newborn mice. Sections in A and B were subjected to immunohistochemistry with the 2H3 antibody against neurofilament protein; those of C and D were stained with hematoxylin and eosin. Arrows indicate the abducens nuclei (an) and the facial nuclei (fn). Dorsal is up. Scale bar, 300 μm.

of the lower teeth in mutant animals suggests that feeding behavior may be impaired. Extensive facial paralysis could also interfere with early feeding proficiency. Consistent with this hypothesis, mutant mice that died shortly after birth did not have milk in their stomachs.

Hoxb-1 mutants lack the facial motor nucleus

Many of the symptoms described above are similar to features seen in humans suffering from Bell's Palsy or Moebius Syndrome (Kumar, 1990), which are associated with damage to or congenital absence of the VIIth (facial) cranial nerve, respectively. In newborn animals, the facial motor nucleus is located in the pons. Sections were made of the head and caudal hindbrain region from five mutant and six control animals . The sections were analyzed either by immunohistochemistry with the 2H3 antibody (Dodd et al., 1988) directed against a subunit of the neurofilament protein (Fig. 3A,B) or by histological staining with hematoxylin and eosin (Fig. 3C,D). In control and mutant animals, the abducens (VIth) nucleus is visible in the dorsomedial aspect of the pons. The large facial motor nucleus is seen at the ventrolateral margin in the sections of wild-type control animals (Fig. 3A,C), but is not visible in the corresponding sections of the *hoxb-1* mutants (B,D). Of the five mutant animals examined, the facial motor nuclei were undetectable in three and severely reduced in the other two. Other histological sections of these animals showed the VIIth as well as the VIIIth (vestibulocochlear) ganglia to be normal in size and shape (data not shown).

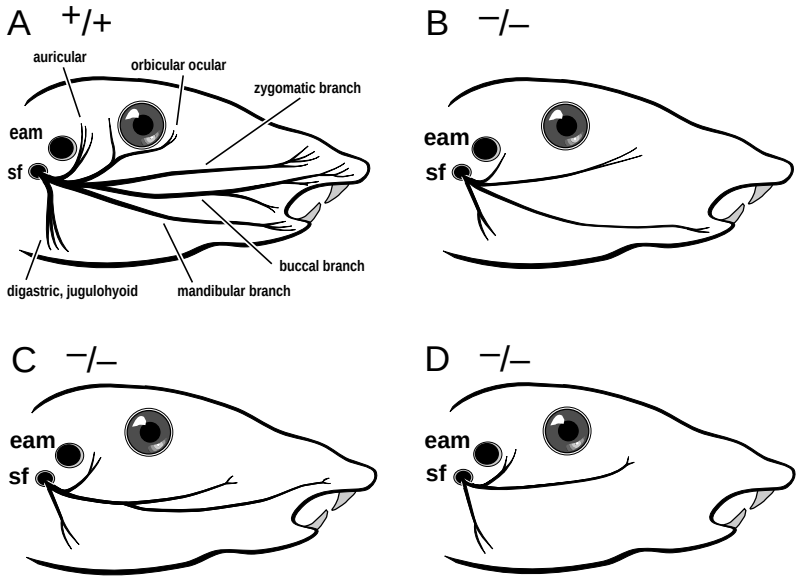

Fig. 4. Schematic diagram illustrating patterns of the facial motor nerve observed in wild-type and *hoxb-1* mutant mice. (B,C) The right and left sides of a *hoxb-1*^{neo} mutant. (D) A second *hoxb-1*^{neo} mutant. Both animals exhibited severe facial paralysis. sf, stylomastoid foramen; eam, external auditory meatus.

Facial nerves and muscles in adult mutant animals

The VIIth nerve is a complex nerve having a sensory, visceromotor and somatic motor component, of which the latter is the most prominent. The somatic motor component controls the muscles of facial expression. Peripherally, the VIIth nerve emerges from the skull through the stylomastoid foramen where the somatic motor component gives rise to six major branches diagrammed in Fig. 4A. In adult animals these branches are readily visible through a dissecting microscope following exposure by surgical dissection of the head and face. Five control animals and six *hoxb-1* homozygous mutant animals were dissected to reveal these nerves and associated muscles (see below). In controls, the pattern of the VIIth motor nerve branches was consistent between animals. However, among the mutant mice the pattern of nerve branches differed from mouse to mouse and even on opposite sides of the same mouse (Fig. 4B-D). All of the nerve branches that could be identified in the *hoxb-1* mutant homozygotes were reduced in diameter approximately 2-3 fold and appeared to terminate prematurely. Several branches were missing, including the branch innervating the orbicularis oris muscle (B,C,D), the mandibular branch (C,D) and the buccal branch (B,D). The mutants shown in Fig. 4 had been scored as having a severe phenotype. One mutant mouse having a less severe phenotype was also dissected. In this animal, all of the major motor nerve branches were detected but reduced, 2-3 fold, in diameter.

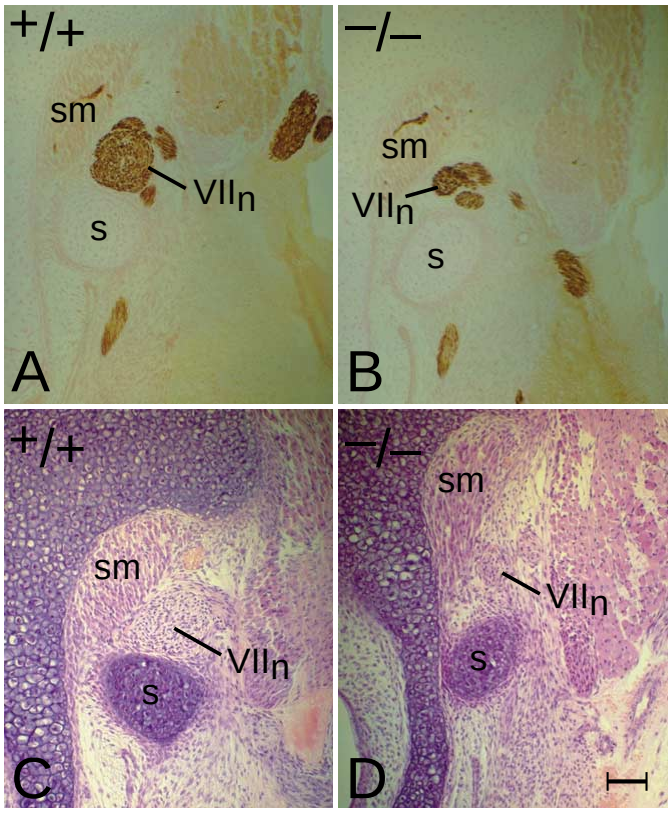

Fig. 5. Innervation of the stapedius muscle in *hoxb-1* mice. Transverse, 10 μm paraffin sections were made of wild-type (A,C) and *hoxb-1*^{neoB} homozygous (B,D) newborn mice. The sections in A and B were subjected to immunohistochemistry with an antibody to neurofilament protein; those in C and D were stained with hematoxylin and eosin. Note the diminished size of the VIIth nerve in B and D. Six heterozygous and five mutant homozygous animals were examined. Dorsal is up. VIIn, VIIth nerve; sm, stapedius muscle; s, stapes. Scale bar, 150 μm.

Although variability in the expressivity of the defects in the VIIth motor nerve branches is evident in these mutant mice, the severity of the defects among survivors did not correlate with the presence of the *hoxb-1*^{neo} or *hoxb-1*^{neoB} mutant alleles.

The sensory component of the VIIth nerve does not appear to be affected by either *hoxb-1* mutation. Sensory neurons, whose cell bodies are located in the VIIth (geniculate) ganglion, innervate taste buds on the soft palate and the anterior two-thirds of the tongue as well as the skin of the external ear. The VIIth ganglion was found to be normal in size and shape in *hoxb-1* mutants when detected either with the 2H3 neurofilament antibody in E10.5 mutant embryos or in histological sections of newborn mutant animals (data not shown). In addition, the density of taste buds, which require innervation for their development, on the anterior two-thirds of the tongue in *hoxb-1* mutants was found to be comparable with those of heterozygotes both in newborn animals (analyzed in histological sections) and in adults (analyzed by microscopy using a camera lucida) (data not shown). The visceromotor or parasympathetic component of the VIIth nerve, however, may be affected by the *hoxb-1* mutation, and these defects may contribute to the loss of viability observed among *hoxb-1*^{neoB} mutant homozygotes following weaning. Parasympathetic neurons innervate the glands of the nasal mucosa and the lacrimal glands through the greater petrosal nerve and the pterygopalatine ganglion, and the salivary glands through the chorda tympani and the submandibular ganglion. The latter neuronal circuit is responsible for activating secretion of saliva following the ingestion of solid food. Interestingly, one of the *hoxb-1* mutant homozygotes that died 15 days after birth showed gross deficiencies of the lacrimal, sublingual and submandibular glands (data not shown).

The faces of *hoxb-1* mutant homozygotes are characteristically narrower than those of their wild-type or heterozygous littermates. The narrowing of the face is apparent two weeks following birth and then becomes progressively more severe with age. Since the skull bones, including the mandible and maxilla, appear normal in *hoxb-1*$^{-}$/*hoxb-1*$^{-}$ mice, the narrowing of the face is most likely a result of facial muscle degeneration. Consistent with this hypothesis is the fact that all of the facial muscles in *hoxb-1* mutant homozygotes appear normal at birth (the facial muscles of three mutant and three control animals were examined in histological, transverse sections). To test for facial muscle integrity in adult animals, the dissections used to expose the branches of the facial nerves, described above, were extended to permit examination of the facial muscles (Table 1). In these *hoxb-1* mutant homozygotes, the zygomatic, buccinator, depressor anguli oris and caudal digastric muscles were reduced approximately two-fold in size compared with those of non-mutant littermates. In both mutants, traces of the nasolabialis muscle could not be found and, in one mutant, the labii maxillaris muscle was not detected. Interestingly, in both mutants, the mass and shape of the temporalis and masseter muscles were abnormal. These muscles are innervated by the Vth cranial nerve. The defects in these muscles most likely arose as an indirect consequence of degeneration of the facial muscles of expression (i.e., abnormal modeling either as a consequence of improper tensions among the facial muscles, decreased usage or both). All of the facial muscles could be detected in a mutant mouse with a less severe phenotype. In this atypical mutant, only the levator nasolabialis and levator labii maxillaris were reduced.

Table 1. Facial muscle patterns in *hoxb-1* mutant mice

Muscle	**hoxb-1*^{neo}	**hoxb-1*^{neo}
platysma	+	+
orbicularis oris	+	+
orbicularis oculi	+	+
jugulohyoid	+	+
zygomatic auricularis	+	+
zygomatic	+/–	+/–
buccinator	+/–	+/–
depressor anguli oris	+/–	+
mentalis	+	+/–
digastric	+/–	+
levator nasolabialis	–	–
levator labii maxillaris	–	+/–
temporalis	+/–	+/–
masseter	+/–	+/–

*Most severe phenotypes, approximately the same age. (+), similar to wild-type in size and shape; (+/–), reduced in size; (–), undetectable. The first group of muscles is innervated by the VIIth nerve; the final two muscles (temporalis and masseter) are innervated by the Vth nerve. All muscles were exposed by surgical dissection.

An additional muscle innervated by the somatic motor component of the VIIth nerve is the stapedius muscle associated with the stapes of the middle ear. The normal function of this muscle is to dampen the movement of the stapes in response to loud noises. In control animals, the stapedius muscle, the stapes and the VIIth nerve are in tight association (Fig. 5A,C). In mutants, the stapes and stapedius muscle appear normal; however, the nerve innervating this muscle is reduced in size and dissociated from the muscle (Fig. 5B,D).

Rhombomere structure, neural crest cell production and neural crest cell migration appear normal in *hoxb-1* mutant mice

The results described above are consistent with the interpretation that the *hoxb-1* phenotype results from defects in the VIIth nerve. However, in mice mutant for the paralogous gene, *hoxa-1*, the neuronal defects result from disorganization of the hindbrain, including the absence of rhombomere 5 (r5) and major defects apparent from r3 through r8 (Carpenter et al., 1993; Mark et al., 1993). Therefore, it was important to examine the integrity of hindbrain organization in the *hoxb-1* mutant mice. In addition, since *hoxb-1* expression is detected in neural crest cells migrating from r4 into the 2nd pharyngeal arch, it was also important to examine mutant mice for defects in the production or migration of r4 neural crest cells or defects in tissues derived from the 2nd pharyngeal arch.

The integrity of rhombomeres in *hoxb-1* mutant mice was examined by the use of a series of molecular markers expressed in the developing hindbrain including *krox-20, hoxb-2, hoxb-3* and *hoxa-2*. *Krox-20* is a zinc-finger transcription factor that is transiently expressed in the early hindbrain in rhombomeres 3 and 5 (Wilkinson et al., 1989a). *Hoxb-1* heterozygous and homozygous mutant E9.0 embryos were subjected to immunohistochemistry with an antibody directed against the krox-20 protein. Production of krox-20 protein in rhombomeres 3 and 5 was indistinguishable in the two embryos (Fig. 6A,E). Thus the r3/r4 and r4/r5 boundaries appear to be intact in the *hoxb-1* mutants. In addition, normal *krox-20*-labelled neural crest

cells, migrating from the hindbrain, were apparent in both embryos.

The expression of *hoxb-2* was examined using RNA in situ hybridization of whole embryos. Fig. 6B,F show results of this analysis in *hoxb-1* heterozygous and homozygous mutant embryos, respectively. No significant differences from controls could be detected in the *hoxb-1* mutant embryo, either in the r2/r3 boundary of *hoxb-2* expression, or in the level of expression in r3, r4 and r5, or in the neural crest migrating from r4 (Wilkinson et al., 1989b; Hunt et al., 1991). This analysis also demonstrated that the *hoxb-1* mutation does not alter the expression pattern of *hoxb-2*, the gene adjacent to *hoxb-1* in the Hox B linkage group. In these preparations, as well as many others, the overall rhombomeric morphology of *hoxb-1* mutant embryos was indistinguishable from that observed in non-mutant embryos. Expression patterns of *hoxa-2* and *hoxb-3* in the hindbrain and neural crest of E9.5 embryos were also found to be similar in *hoxb-1* control and mutant embryos (data not shown).

The pattern of neural crest migration from rhombomere 4 was further examined by two additional means. First, *hoxb-1* heterozygous and homozygous mutant E9.0 embryos were examined by immunohistochemistry with an antibody against the CRABP1 protein, which labels neural crest cells migrating from rhombomeres 2, 4 and 6 (Maden et al., 1992). In the heterozygous control embryo (Fig. 6C), a stream of neural crest cells migrating from rhombomere 4 into the second pharyngeal arch is seen. A similar pattern of migration is present in the homozygous mutant embryo (Fig. 6G).

The second method used to examine neural crest from rhombomere 4 involved introducing DiI into the neural tube of *hoxb-1* heterozygous and homozygous mutant E8.5 embryos and analyzing the migration of the resulting DiI-labelled neural crest after 24 hours of in vitro culture (Serbedzija et al., 1992; Manley and Capecchi, 1995). Examples of this type of analysis are shown in Fig. 6D,H. Again, one can see a stream of neural crest cells migrating from rhombomere 4 in both the heterozygous and homozygous mutant embryos. Finally, *hoxb-1* mutant mice were carefully examined for defects in tissues and

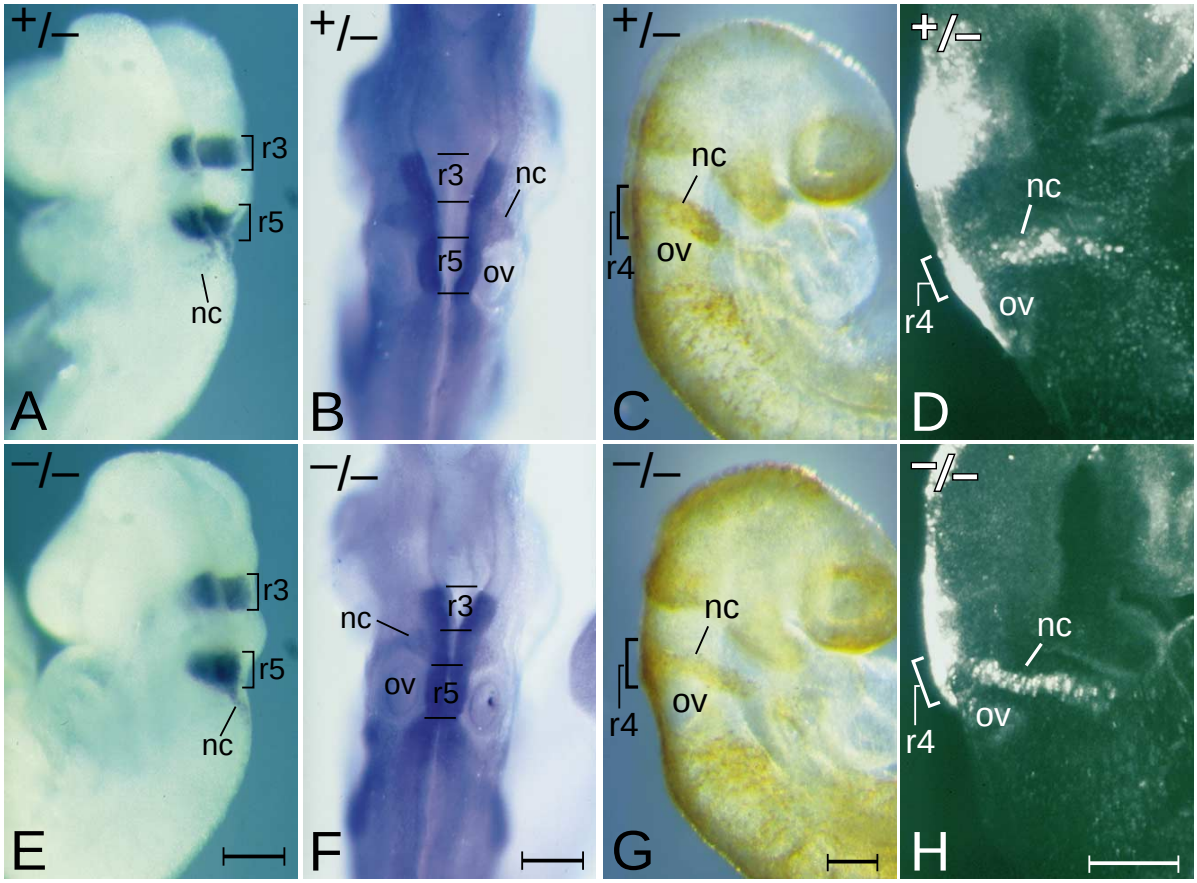

Fig. 6. Hindbrain structure, marker-gene expression patterns and cranial neural crest in *hoxb-1* embryos. (A,E) Dorsolateral views of *hoxb-1^{neoB}* heterozygous (A) and homozygous (E) E8.5 embryos subjected to immunohistochemistry with an antibody directed against the krox-20 protein. (B,F) Dorsal views of *hoxb-1^{neoB}* heterozygous (B) and mutant (F) E9.5 embryos that were hybridized with a digoxigenin-labelled *hoxb-2* probe. (C,G) Lateral views of *hoxb-1^{neoB}* heterozygous (C) and homozygous (G) E9.0 embryos that had been incubated with an antibody against the CRA BP1 protein. The lines indicate the stream of r4-derived neural crest cells migrating into pharyngeal arch 2. (D,H) Lateral views of E8.5 embryos that had been labelled by amniotic cavity injection of DiI, cultured for 24 hours and analyzed by confocal microscopy. (D) Heterozygous *hoxb-1^{neo}* embryo with labelled neural crest cells migrating from r4 to arch 2. (H) *hoxb-1^{neo}* homozygous mutant embryo with r4 neural crest labelled. For *krox-20* staining, two heterozygous and two homozygous mutant *hoxb-1^{neoB}* embryos were examined. Analysis with the *hoxb-2* probe included four heterozygous (*1 hoxb-1^{neo}, 3 hoxb-1^{neoB}*) and four homozygous mutants (1 *hoxb-1^{neo}*, 3 *hoxb-1^{neoB}*). Staining with the CRABP 1 antibody was performed on one heterozygous and two homozygous mutant *hoxb-1^{neoB}* embryos. The DiI-labelled neural crest was observed in three heterozygous and one mutant *hoxb-1^{neo}* embryos and in two heterozygous and one mutant *hoxb-1^{neoB}* embryos. Anterior is up. nc, neural crest; ov, otic vesicle; scale bars for C and G, 130 μm; for all other panels, 200 μm.

bones derived from r4-mesenchymal neural crest cells but none was observed (data not shown).

Development of the facial nerve

The position and early migration patterns of the cell bodies in the hindbrain associated with the VIIth nerve can be determined by retrograde labelling of these cells with fluorescent carbocyanine dyes. We previously described (Carpenter et al., 1993) the distribution of efferent neurons in the hindbrain of E11.5 wild-type embryos following injection of DiI into the VII/VIIIth (facial/vestibulocochlear) cranial ganglion complex to label neurons in r4 and r5, and injection of a second carbocyanine dye, DiO, into the Vth (trigeminal) cranial ganglion to label neurons in r1-3. Results from control embryos double-labelled in this way are shown in Fig. 7. Since rhombomere boundaries are no longer clearly visible at E11.5, the DiO-labelling patterns in rhombomeres 1-3 define the level of the r3/r4 boundary. Fig. 7A shows the ventral surface of the right side of the control hindbrain that was photographed with fluorescein optics, which allows viewing of both DiI and DiO. In Fig. 7B, the same hindbrain was photographed with a rhodamine filter which allows visualization only of DiI. In this figure, one can see the typical 'fan-shaped' pattern formed by the cell bodies and their fibers in rhombomeres 4 and 5. Axons from the medial cell bodies in rhombomere 4 extend laterally, exiting the hindbrain at the level of rhombomere 4 in tightly bound fascicles. In rhombomere 5 there are two populations of neurons. First, there is a medial group whose cell bodies are adjacent to the ventral midline and whose axons project anteriorly and then laterally. These cells are likely to contribute to the facial motor nucleus. The second group has more laterally positioned cell bodies and projects axons laterally and then anterolaterally. Fibers from both populations exit the hindbrain at the level of rhombomere 4. The more lateral population of neurons in rhombomere 5 is likely to contribute to the parasympathetic preganglionic cells that will form the superior salivatory and lacrimal nuclei just caudal to the facial motor nucleus in the pons.

Many of the medial cell bodies in r4 and r5 appear to be migrating caudally and then ventrolaterally. Details of this migration pattern are more apparent at higher magnification. Migrating cells extend leading processes in the direction of their migration, and then elongate their cell bodies along the same direction. Such leading processes and their migrating cell bodies can be seen in Fig. 7E (elongated migrating cells and their fibers are indicted by the arrows in Fig. 7C-E).

DiO and DiI were also injected into the cranial ganglia of *hoxb-1* homozygous mutant embryos. Fig. 8A,B show the ventral surface of the right side of a *hoxb-1* mutant hindbrain injected with DiO in the Vth ganglion (GV) and DiI into the VII/VIIIth complex. Cell bodies associated with GV efferent neurons are again restricted to r1-3, while those projecting axons to the GVII complex are present in r4,5. Thus, rhombomere integrity appears to be intact in the mutant embryos. This is in contrast to *hoxa-1* mutant embryos in which rhombomere 5 is missing and the efferent neurons labelled by injection of DiI into the VIIth ganglion are detected anteriorly as far as r3 and posteriorly as far as r8 (Carpenter et al., 1993).

Fig. 8D-F shows the DiI-labelling patterns in rhombomeres 4 and 5 in three additional *hoxb-1* mutant embryos. The most striking feature common to the mutant embryos is that the neurons normally present along the medial margin of r4 and r5 are either absent, greatly reduced in number, or different in character. Anteriorly directed axon fibers could not be detected from the medial cell bodies in either rhombomere 4 or 5. Furthermore, neuronal cell bodies are observed to be dispersed more laterally in rhombomere 4 and appear to be migrating laterally. The identity of these neurons is not known. Finally, the fibers in

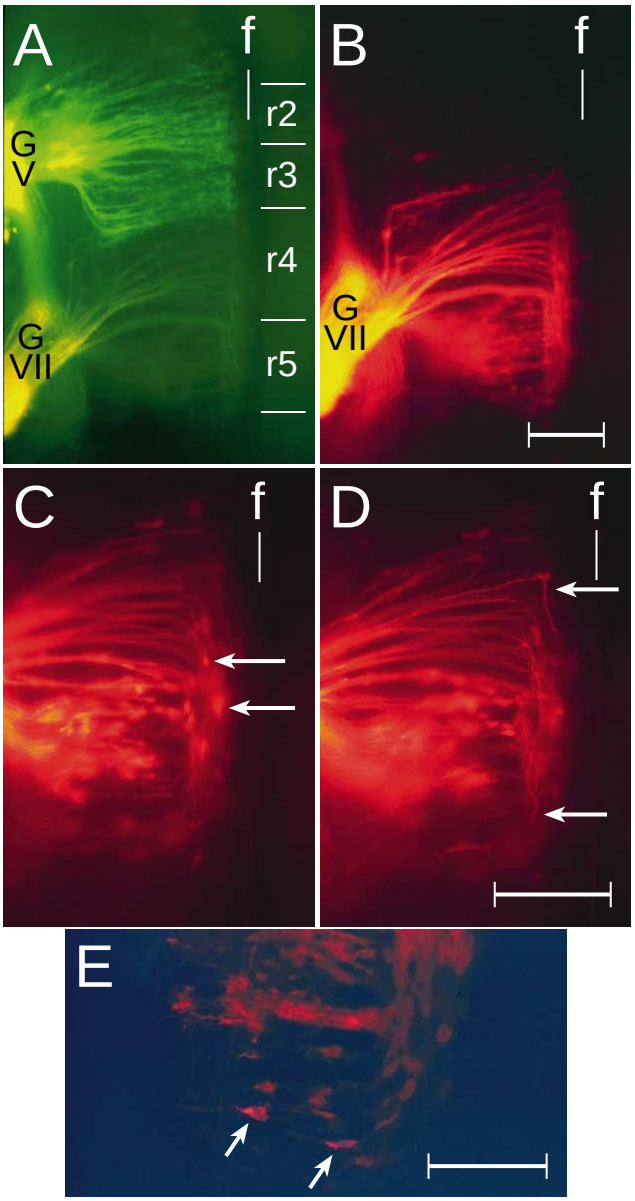

Fig. 7. Retrograde labelling of the hindbrains of wild-type or *hoxb-1* heterozygous embryos. Unilateral, ventral views of the hindbrains of E11.5 embryos are shown following retrograde labelling with DiO and DiI. (A) An embryo injected with DiO in the Vth cranial ganglion (GV) and DiI in the VIIth cranial ganglion (GVII), and photographed with a fluorescein filter. (B) The same field as in A, but using a rhodamine filter. Note the typical 'fan-shaped' pattern of neuron cell bodies and their axons in r4 and r5. (C,D) Two focal planes, using rhodamine optics, of a second embryo showing migrating medial cells and their axons (arrows). (E) A confocal image showing more detail of the migrating neurons (arrows) in the caudal region of r5. Anterior is up. Vertical white line, labelled f, indicates the floor plate. Scale bars for A,B and C,D, 200 μm; for E, 100 μm.

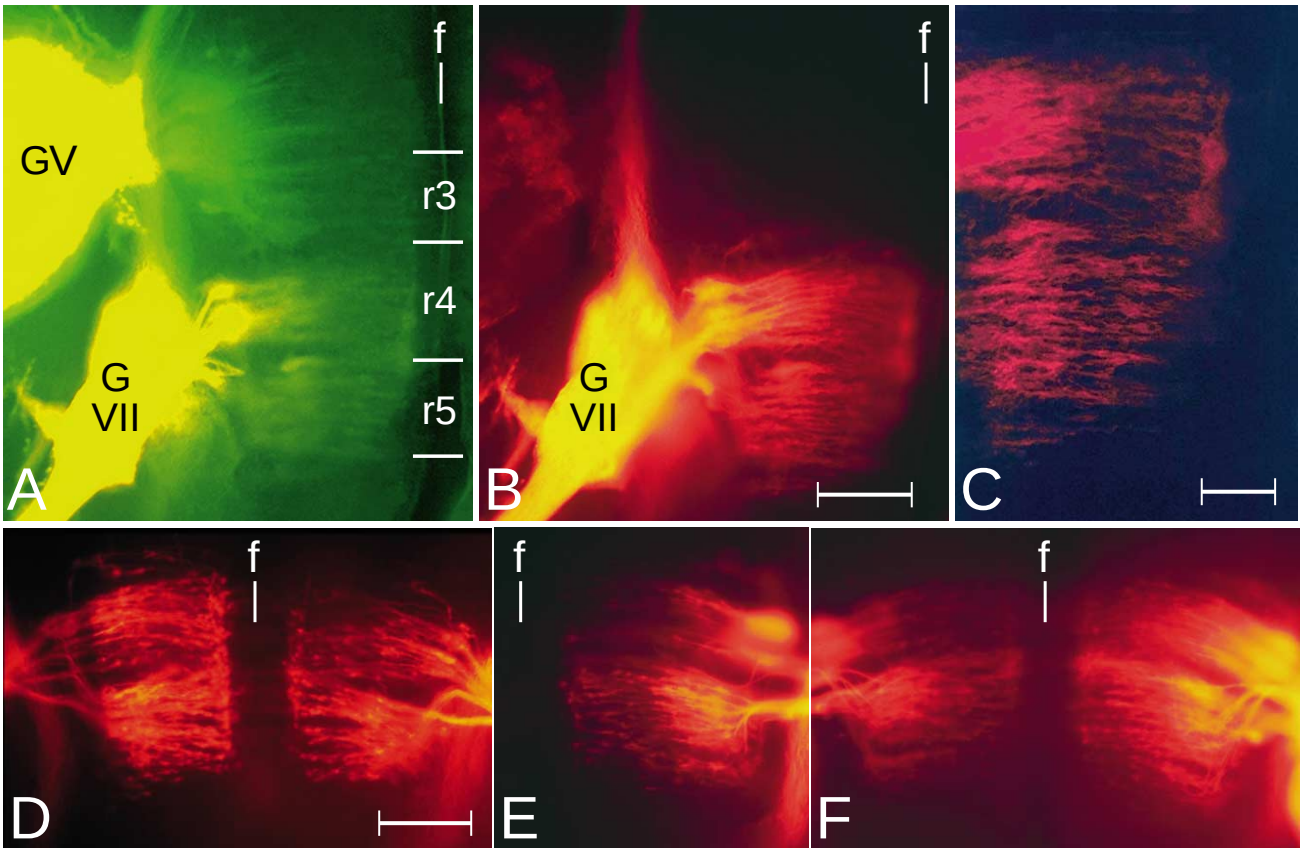

Fig. 8. Ventral views of the hindbrains of E11.5 *hoxb-1* mutant embryos after retrograde labelling with DiI and DiO. (A,B) the right side of a *hoxb-1*^{neoB} embryo injected with DiO and DiI in GV and GVII, respectively, and viewed under fluorescein (A) or rhodamine (B) optics. (C) confocal image of the more medial aspect of the r4/r5 region of the embryo shown in B. (D-F) The r4/r5 region of three additional *hoxb-1* mutant embryos injected in GVII with DiI and viewed under rhodamine optics. Note the absence of the'fan-shaped' pattern in all embryos, and the scarcity of r4 neurons in E and F, left side. For the *hoxb-1*^{neo} allele, two heterozygous and two homozygous mutant embryos were examined; for the *hoxb-1*^{neoB} allele, nine heterozygous and eight homozygous mutant embryos were analyzed. The *hoxb-1* genotypes of the embryos shown in (D-F) are *neo/neo*, *neoB/neoB* and *neoB/neoB*, respectively. GV, GVII, and f are as described for Fig. 7. Scale bars for A,B and D,E,F, 200 μm; for C, 100 μm.

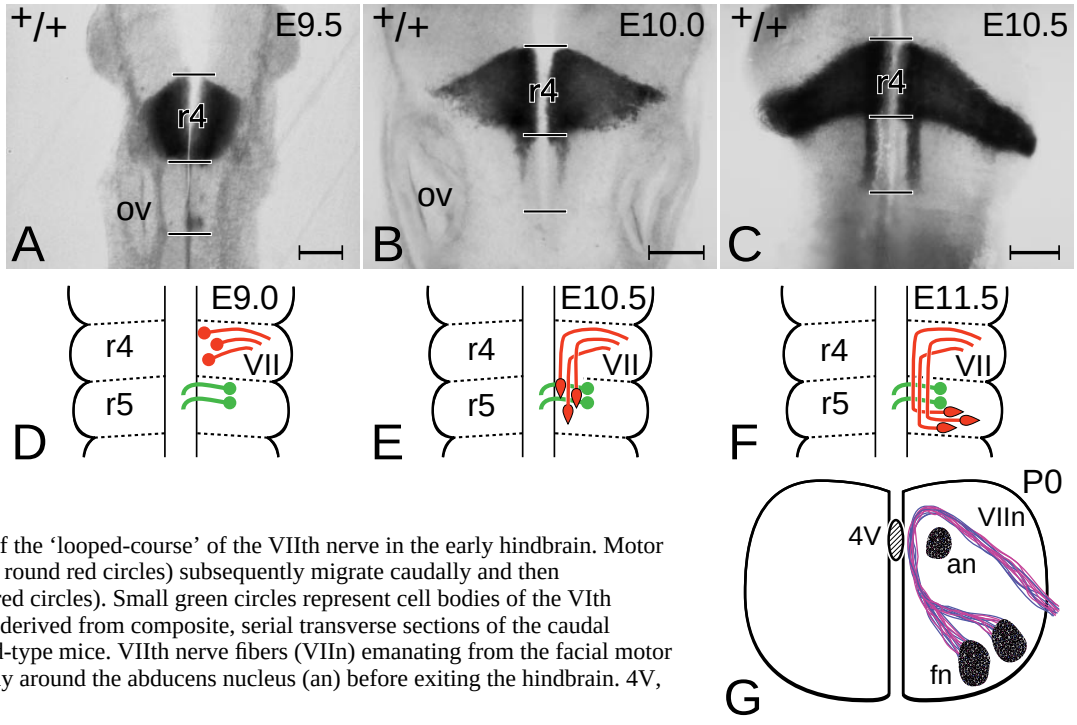

Fig. 9. Development and specification of facial motor neurons. (A-C) Coronal, vibratome sections (200 μm) of SWR/J embryos immunostained with an antibody against hoxb-1 protein. Note the increase in medial staining in the anterior region of r5 between E10.0 (B), and E10.5 (C). Anterior is up. ov, otic vesicle. Scale bar in A, 100 μm; those in B and C, 200 μm. (D-F) Schematic diagram illustrating the origin of the 'looped-course' of the VIIth nerve in the early hindbrain. Motor neurons born medially in r4 (D, round red circles) subsequently migrate caudally and then ventrolaterally (E,F, elongated red circles). Small green circles represent cell bodies of the VIth (abducens) nerve. (G) Diagram derived from composite, serial transverse sections of the caudal hindbrain of newborn (PO) wild-type mice. VIIth nerve fibers (VIIn) emanating from the facial motor nucleus (fn) travel dorsomedially around the abducens nucleus (an) before exiting the hindbrain. 4V, 4th ventricle.

rhombomere 4 of the mutant embryos exit the hindbrain without forming the tightly bound fascicles seen in control embryos. Fig. 8C shows a higher magnification of the embryo in B emphasizing the lack of caudal and ventrolateral migration of the medial neurons around the parasympathetic neurons in rhombomere 5.

Whether the pattern of parasympathetic preganglionic neurons in rhombomere 5 is affected by the *hoxb-1* mutation is more difficult to discern. Examination of this component shows it to be less robust and more diffuse in mutants than in controls. Also the cell bodies, especially those of the embryo shown in Fig. 8D, appear to extend more medially, possibly because they are not displaced by migrating medial motor neurons. DiI was also injected in the IXth (glossopharyngeal) and Xth (nodose) cranial ganglia in 4 *hoxb-1* mutant homozygous embryos. The resulting labelling patterns in r6-8 were indistinguishable from those of non-mutant animals.

Origin of the facial motor neurons

In the absence of *hoxb-1*, formation of the facial motor neurons is severely affected, suggesting that the hoxb-1 gene product is required for specification of these neurons. Although the penetrance of the phenotype is 100%, some variation in expressivity is apparent, suggesting that other *Hox* genes may compensate for this function. Between E9.0 and E9.5, *hoxb-1* expression in the rostral portion of the embryo is restricted to rhombomere 4 (Fig. 9A). At E10.0 a medial finger of *hoxb-1* expression begins to be extended caudally into r5 and becomes more pronounced by E10.5 (Fig. 9B-C). A similar pattern of hoxb-1 expression in r5 has been observed in E10.5 transgenic mice which contained a *lacZ* reporter gene (Marshall et al., 1992). The dynamics of *hoxb-1* expression in normal embryos suggest that the facial motor neurons are first specified in r4 and then migrate caudally along the medial axis into r5. On reaching the r5/r6 boundary these neurons turn abruptly and migrate laterally (see Fig. 7). This migration pattern is diagrammed in Fig. 9D-F. Consistent with the hypothesis that the facial motor neurons are generated in r4, Lumsden and Keynes (1989) have previously noted that, in the hindbrain, neuron maturation occurs earlier in even-numbered rhombomeres than in odd-numbered rhombomeres. Also, mice mutant for *krox-20*, which are deficient in the formation and/or maintenance of rhombomeres 3 and 5, have a morphologically normal facial motor nucleus (Schneider-Maunoury et al., 1993).

The somatic motor component of the VIIth nerve is characterized by its unusual 'looped' course through the pons (Altman and Bayer, 1982). Thus, although the motor nucleus is located ventrolaterally in the pons, its axons project dorsomedially around the VIth (abducens) nuclei and then turn ventrolaterally to exit the pons (diagrammed in Fig. 9G). The course of this loop can be understood in terms of the early migration pattern of these neurons during development proposed here (Fig. 9D-F).

DISCUSSION

We generated mice with two separate targeted disruptions of *hoxb-1*. The first, *hoxb-1*^{neo}, disrupts the homeodomain, and the second, *hoxb-1*^{neoB}, disrupts the first exon of *hoxb-1*, as well as the homeodomain. Among survivors, phenotypes of mice homozygous for the two mutant alleles were not distinguishable, arguing that the homeodomain, which confers DNA-binding capability, is an essential component of *hoxb-1* protein function. However, mutants for the *hoxb-1*^{neoB} allele did show greater morbidity at birth and at the age of weaning, suggesting that this mutation is a more severe loss-of-function allele.

The inability to distinguish these two mutant alleles among survivors may result from both mutant alleles showing similar variability in the expressivity of the mutant phenotype, thereby masking their differences. This variability is likely to result from overlap of function from other *Hox* genes. At least two *Hox* genes can provide compensation for the *hoxb-1* mutation, *hoxa-1* and *hoxb-2*. Thus, mice mutant for both *hoxa-1* and *hoxb-1* show a very exacerbated *hoxb-1* mutant phenotype (Rossel and Capecchi, unpublished results). Similarly, mice expressing neither *hoxb-1* nor *hoxb-2* show a stronger and less variable *hoxb-1* mutant phenotype than do *hoxb-1*^{neoB} homozygotes (Barrow and Capecchi, unpublished data).

The predominant feature of the *hoxb-1* mutant homozygous phenotype among survivors is paralysis of the muscles controlling facial expression. This feature is also observed in humans suffering from Bell's Palsy or Moebius Syndrome. These human diseases result from damage to, or congenital absence of, the VIIth (facial) cranial nerve, respectively. *Hoxb-1* mutant homozygotes also have defects in the VIIth nerve. Thus, sections of the pons show a marked reduction or absence of the VIIth nerve motor nucleus. Also, surgical examination of the facial periphery shows that the major VIIth nerve somatic motor branches are either absent or reduced 2-3 fold in diameter. Finally, at E11.5 retrograde labelling of neurons in *hoxb-1* mutant hindbrains by injection of DiI into the VII/VIIIth ganglionic complex fails to label cells thought to give rise to the VIIth nerve motor nucleus.

The entire *hoxb-1* phenotype could be explained in terms of a defect in the formation of the VIIth nerve. This interpretation would postulate that the primary role of *hoxb-1* is to specify the neurons that will form the somatic motor component of the VIIth nerve. Consistent with this hypothesis, we have not observed any defects in tissues or structures derived from neural crest cells in *hoxb-1* mutant mice or from the 2nd pharyngeal arch, both sites of *hoxb-1* expression. The rhombomeric pattern of the embryonic hindbrain also appears normal. This is in sharp contrast to *hoxa-1* mutant mice, which exhibit gross defects in the metameric organization of the hindbrain (Carpenter et al., 1993; Mark et al., 1993; Capecchi, 1997).

Whether the *hoxb-1* mutation affects other components of the VIIth nerve is less clear. The sensory component does not appear to be affected since both the VIIth ganglion and taste buds on the anterior two-thirds of the tongue appear normal in *hoxb-1* mutant homozygotes. On the contrary, the parasympathetic component of the VIIth nerve may be affected in these mutant mice, but changes in this component show incomplete penetrance and broad variability in expressivity. A number of survivors have been examined histologically for defects in the lacrimal, sublingual and submandibular glands and none were observed. However, a *hoxb-1* mutant homozygote that died 15 days after birth had gross defects in these glands. The morbidity of *hoxb-1*^{neoB} homozygotes following their transfer to solid foods could be explained in terms of defects in the parasympathetic component of the VIIth nerve.

Hoxb-1 mutant mice have narrow faces relative to control

littermates. This phenotype becomes apparent two weeks after birth and then becomes progressively more severe with age. Since the skull bones in these mutant mice appear normal, this defect has been attributed to facial muscle degeneration. Consistent with this hypothesis, we found that a number of facial muscles either had reduced mass or could not be detected in *hoxb-1* adult mutant mice but were histologically normal in mutant newborn animals. However, we were surprised that there was not complete degeneration of the facial muscles. Survival of the remaining facial muscle fibers may result from more extensive arborization of the remaining VIIth nerve fibers, from abnormal innervation by other cranial nerves (i.e., the Vth or IXth nerve) or both.

Hoxb-1 mutant mice fail to form the VIIth nerve motor nucleus. The fate of the cells that, in the presence of hoxb-1 protein, would normally give rise to these motoneurons has not been determined in mutant embryos. They may fail to proliferate or they may die. Alternatively, they may have acquired a new fate. Injection of DiI into the VII/VIIIth ganglionic complex of *hoxb-1* mutant mice labels nuclei in the more lateral aspect of rhombomere 4 that are not observed in control wild-type or heterozygous embryos. The identity of these cells has not been determined. However, they send axons to the VII/VIIIth ganglionic complex. Determination of whether these cells represent cells with an altered fate or an altered motoneuron behavior must await further experimentation.

The differences in phenotype between mice with targeted disruptions in the two paralogous genes *hoxa-1* and *hoxb-1* are extensive. At E8.0 both genes have the same anterior limit of expression at the presumptive r3/r4 rhombomere boundary. However, whereas *hoxa-1* expression rapidly recedes, such that by E8.5 *hoxa-1* expression is no longer detectable in the hindbrain, *hoxb-1* expression remains behind in a stripe of expression in presumptive rhombomere 4 (Murphy and Hill, 1991). This expression is upregulated in rhombomere 4 and maintained via autoregulation well into mid-gestation (Pöpperl et al., 1995). As already mentioned, in the absence of *hoxa-1* function, hindbrain development is severely affected, rhombomere 5 is missing and defects are apparent from rhombomere 3 through rhombomere 8. The phenotype suggests either that rhombomere 5 is not formed or not maintained. Such a role in segmentation is in contrast to the situation in *Drosophila*, in which mutations in *HomC* genes do not alter the pattern of segmentation but rather determine the identity of cells within parasegments. On the contrary, the *hoxb-1* mutation does not alter the rhombomere pattern but rather appears to alter the fate of a restricted set of cells within rhombomere 4. In this sense *hoxb-1* function parallels more closely the function of *HomC* genes in *Drosophila*.

In summary, mice mutant for *hoxb-1* have defects in the formation of the somatic motor component of the VIIth (facial) nerve. The abnormality appears to result from a defect in cell specification. The analysis of these mutant mice has provided a model for when and where these motor neurons are specified and for how the early migration patterns in the developing hindbrain lead to the circuitous axonal projection that typifies the facial motor nucleus in the pons. The phenotype of *hoxb-1* mutant mice resembles symptoms found in humans with Bell's Palsy or Moebius Syndrome. These mutant mice may allow study of the etiology of these diseases in greater detail than is possible in humans as well as serve as a model for developing more effective therapies.

We especially acknowledge and thank J. Barrow for his many contributions to this work, including in situ hybridization and immunostaining of vibratome sections. B. Condie prepared the *krox-20* GST-fusion construct used to generate the *krox-20* antisera and K. Thomas provided DNA vectors. We thank E. Carpenter for help with neuroanatomy, M. Allen, C. Lenz, G. Peterson, S. Barnett, E. Nakashima and M. Wagstaff for excellent technical assistance, and L. Oswald for help with preparation of the manuscript. The CRABP 1 antibody was generously provided by U. Eriksson. The 2H3 neurofilament hybridoma was obtained from the Developmental Studies Hybridoma Bank under contract N01-HD-6-2915 from the NICHD.

REFERENCES

Altman, J. and Bayer, S. (1982). Development of the cranial nerve ganglia and related nuclei in the rat. In *Advances in Anatomy, Embryology and Cell Biology*, **74**, pp. 1-90. New York: Springer-Verlag.

Beck, E., Ludwig, G., Auserwald, E. A., Reiss, B. and Schaller, H. (1982). Nucleotide sequence and exact localization of the neomycin phosphotransferase gene from transposon Tn5. *Gene* **19**, 327-336.

Boulet, A. M. and Capecchi, M. R. (1996). Targeted disruption of *hoxc-4* causes esophageal defects and vertebral transformations. *Dev. Biol.* **177**, 232-249.

Capecchi, M. R. (1997). The role of *Hox* genes in hindbrain development. In *Molecular and Cellular Aspects of Neural Development.* (ed.W. M. Cowan, T. M. Jessell and S. L. Zipursky), New York: Oxford University Press. In press.

Carpenter, E. M., Goddard, J. M., Chisaka, O., Manley, N. R. and Capecchi, M. R. (1993). Loss of *Hox-A1* (*Hox-1.6*) function results in the reorganization of the murine hindbrain. *Development* **118**, 1063-1075.

Chisaka, O. and Capecchi, M. R. (1991). Regionally restricted developmental defects resulting from targeted disruption of the mouse homeobox gene *hox-1.5*. *Nature* **350**, 473-479.

Chisaka, O., Musci, T. S. and Capecchi, M. R. (1992). Developmental defects of the ear, cranial nerves and hindbrain resulting from targeted disruption of the mouse homeobox gene *Hox-1.6*. *Nature* **355**, 516-520.

Davis, A. P. and Capecchi, M. R. (1994). Axial homeosis and appendicular skeleton defects in mice with a targeted disruption of *hoxd-11*. *Development* **120**, 2187-2198.

Davis, A. P., Witte, D. P., Hsieh-Li, H. M., Potter, S. S. and Capecchi, M. R. (1995). Absence of radius and ulna in mice lacking *hoxa-11* and *hoxd-11*. *Nature* **375**, 791-795.

Davis, A. P. and Capecchi, M. R. (1996). A mutational analysis of the 5′ Hox D genes: Dissection of genetic interactions during limb development in the mouse. *Development* **122**, 1175-1185.

Dodd, J., Morton, S. B., Karagogeos, D., Yamamoto, M. and Jessell, T. M. (1988). Spatial regulation of axonal glycoprotein expression on subsets of embryonic spinal neurons. *Neuron* **1**, 105-116.

Dollé, P., Izpisúa-Belmonte, J.-C., Falkenstein, H., Renucci, A. and Duboule, D. (1989). Coordinate expression of the murine *Hox-5* complex homeobox-containing genes during limb pattern formation. *Nature* **342**, 767-772.

Dollé, P., Izpisúa-Belmonte, J.-C., Boncinelli, E. and Duboule, D. (1991). The *Hox-4.8* gene is localized at the 5′ extremity of the *Hox-4* complex and is expressed in the most posterior parts of the body during development. *Mech. Dev.* **36**, 3-13.

Dollé, P., Dierich, A., LeMeur, M., Schimmang, T., Schuhbaur, B., Chambon, P. and Duboule, D. (1993). Disruption of the *Hoxd-13* gene induces localized heterochrony leading to mice with neotenic limbs. *Cell* **75**, 431-441.

Duboule, D. and Dollé, P. (1989). The structural and functional organization of the murine *Hox* gene family resembles that of *Drosophila* homeotic genes. *EMBO J.* **8**, 1497-1505.

Eriksson, U., Hansson, E., Nordlinder, H., Busch, C., Sundelin, J. and Peterson, P. A. (1987). Quantitation and tissue localization of the cellular retinoic acid-binding protein. *J. Cell. Physiol.* **133**, 482-490.

Favier, B., Rijli, F. M., Fromental-Ramain, C., Fraulob, V. and Chambon, P. (1996). Functional cooperation between the non-paralogous genes *Hoxa-*

10 and *Hoxd-11* in the developing forelimb and axial skeleton. *Development* **122**, 449-460.

Frohman, M. A., Boyle, M. and Martin, G. R. (1990). Isolation of the mouse *Hox-2.9* gene; analysis of embryonic expression suggests that positional information along the anterior-posterior axis is specified by mesoderm. *Development* **110**, 589-607.

Fromental-Ramain, C., Warot, X., Lakkaraju, S., Favier, B., Haack, H., Birling, C., Dierich, A., Dollé, P. and Chambon, P. (1996). Specific and redundant functions of the paralogous *Hoxa-9* and *Hoxd-9* genes in forelimb and axial skeleton patterning. *Development* **122**, 461-472.

Gendron-Maguire, M., Mallo, M., Zhang, M. and Gridley, T. (1993). *Hoxa-2* mutant mice exhibit homeotic transformation of skeletal elements derived from cranial neural crest. *Cell* **75**, 1317-1331.

Graham, A., Papalopulu, N. and Krumlauf, R. (1989). The murine and *Drosophila* homeobox gene complexes have common features of organization and expression. *Cell* **57**, 367-378.

Horan, G. S. B., Ramírez-Solis, R., Featherstone, M. S., Wolgemuth, D. J., Bradley, A. and Behringer, R. R. (1995). Compound mutants for the paralogous *hoxa-4*, *hoxb-4*, and *hoxd-4* genes show more complete homeotic transformations and a dose-dependent increase in the number of vertebrae transformed. *Genes Dev.* **9**, 1667-1677.

Hunt, P., Gulisano, M., Cook, M., Sham, M.-H., Faiella, A., Wilkinson, D., Boncinelli, E. and Krumlauf, R. (1991). A distinct *Hox* code for the branchial region of the vertebrate head. *Nature* **353**, 861-864.

Izpisúa-Belmonte, J,-C., Falkenstein, H., Dollé, P., Renucci, A. and Duboule, D. (1991). Murine genes related to the *Drosophila AbdB* homeotic gene are sequentially expressed during development of the posterior part of the body. *EMBO J.* **10**, 2279-2289.

Jeannotte, L., Lemieux, M., Charron, J., Poirier, F. and Robertson, E. J. (1993). Specification of axial identity in the mouse: role of the *Hoxa-5* (*Hox-1.3*) gene. *Genes Dev.* **7**, 2085-2096.

Kostic, D. and Capecchi, M. R. (1994). Targeted disruptions of the murine *hoxa-4* and *hoxa-6* genes result in homeotic transformations of components of the vertebral column. *Mech. Dev.* **46**, 231-247.

Kumar, D. (1990). Moebius syndrome. *J. Med. Genet.***27**, 122-126.

LeMouellic, H., Lallemand, Y. and Brûlet, P. (1992). Homeosis in the mouse induced by a null mutation in the *Hox-3.1* gene. *Cell* **69**, 251-264.

Lewis, E. B. (1978). A gene complex controlling segmentation in *Drosophila*. *Nature* **276**, 565-570.

Lufkin, T., Dierich, A., LeMeur, M., Mark, M. and Chambon, P. (1991). Disruption of the *Hox-1.6* homeobox gene results in defects in a region corresponding to its rostral domain of expression. *Cell* **66**, 1105-1119.

Lumsden, A. and Keynes, R. (1989). Segmental patterns of neuronal development in the chick hindbrain. *Nature* **337**, 424-428.

Maden, M., Horton, C., Graham, A., Leonard, L., Pizzey, J., Siegenthaler, G., Lumsden, A. and Eriksson, U. (1992). Domains of cellular retinoic acid-binding protein I (CRA BP I) expression in the hindbrain and neural crest of the mouse embryo. *Mech. Dev.* **37**, 13-23.

Manley, N. R. and Capecchi, M. R. (1995). The role of *hoxa-3* in mouse thymus and thyroid development. *Development* **121**, 1989-2003.

Mansour, S. L., Thomas, K. R. and Capecchi, M. R. (1988). Disruption of the proto-oncogene *int-2* in mouse embryo-derived stem cells: a general strategy for targeting mutations to non-selectable genes. *Nature* **336**, 348-352.

Mansour, S. L., Goddard, J. M. and Capecchi, M. R. (1993). Mice homozygous for a targeted disruption of the proto-oncogene *int-2* have developmental defects in the tail and inner ear. *Development* **117**, 13-28.

Mark, M., Lufkin, T., Vonesch, J.-L., Ruberte, E., Olivo, J.-C., Dollé, P., Gorry, P., Lumsden, A. and Chambon, P. (1993). Two rhombomeres are altered in *Hoxa-1* mutant mice. *Development* **119**, 319-338.

Marshall, H., Nonchev, S., Sham, M. H., Muchamore, I., Lumsden, A. and Krumlauf, R. (1992). Retinoic acid alters hindbrain Hox code and induces transformation of rhombomeres 2/3 into a 4/5 identity. *Nature* **360**, 737-741.

Murphy, P. and Hill, R. E. (1991). Expression of the mouse *labial*-like homeobox-containing genes, *Hox-2.9* and *Hox-1.6*, during segmentation of the hindbrain. *Development* **111**, 61-74.

Nagy, A., Rossant, J., Nagy, R., Abramow-Newerly, W. and Roder, J. C. (1993). Derivation of completely cell culture-derived mice from early-passage embryonic stem cells. *Proc. Natl. Acad. Sci. USA* **90**, 8424-8428.

Pöpperl, H., Bienz, M., Studer, M., Chan, S.-K., Aparicio, S., Brenner, S., Mann, R. S. and Krumlauf, R. (1995). Segmental expression of *Hoxb-1* is controlled by a highly conserved autoregulatory loop dependent upon *exd/pbx*. *Cell* **81**, 1031-1042.

Ramirez-Solis, R., Zheng, H., Whiting, J., Krumlauf, R. and Bradley, A. (1993). *Hoxb-4* (*Hox-2.6*) mutant mice show homeotic transformation of a cervical vertebra and defects in the closure of the sternal rudiments. *Cell* **73**, 279-294.

Rancourt, D. E., Tsuzuki, T. and Capecchi, M. R. (1995). Genetic interaction between *hoxb-5* and *hoxb-6* is revealed by nonallelic noncomplementation. *Genes Dev.* **9**, 108-122.

Rijli, F. M., Mark, M., Lakkaraju, S., Dierich, A., Dollé, P. and Chambon, P. (1993). A homeotic transformation is generated in the rostral branchial region of the head by disruption of *Hoxa-2*, which acts as a selector gene. *Cell* **75**, 1333-1349.

Roberts, D. J., Johnson, R. L., Burke, A. C., Nelson, C. E., Morgan, B. A. and Tabin, C. (1995). Sonic hedgehog is an endodermal signal inducing *Bmp-4* and *Hox* genes during induction and regionalization of the chick hindgut. *Development* **121**, 3163-3174.

Satokata, I., Benson, G. and Maas, R. (1995). Sexually dimorphic sterility phenotypes in *Hoxa10*-deficient mice. *Nature* **374**, 460-463.

Schneider-Maunoury, S., Topilko, P., Seitanidou, T., Levi, G., Cohen-Tannoudji, M., Pournin, S., Babinet, C. and Charnay, P. (1993). Disruption of *Krox-20* results in alteration of rhombomeres 3 and 5 in the developing hindbrain. *Cell* **75**, 1199-1214.

Serbedzija, G. N., Bronner-Fraser, M. and Fraser, S. E. (1992). Vital dye analysis of cranial neural crest cell migration in the mouse embryo. *Development* **116**, 297-307.

Small, K. M. and Potter, S. S. (1993). Homeotic transformations and limb defects in *HoxA-11* mutant mice. *Genes Dev.* **7**, 2318-2328.

Smith, D. B. and Johnson, K. S. (1988). Single-step purification of polypeptides expressed in *Escherichia coli* as fusions with glutathione S-transferase. *Gene* **67**, 31-40.

Suemori, W., Takahashi, N. and Noguchi, S. (1995). *Hoxc-9* mutant mice show anterior transformation of the vertebrae and malformation of the sternum and ribs. *Mech. Dev.* **51**, 265-273.

Thomas, K. R. and Capecchi, M. R. (1987). Site-directed mutagenesis by gene targeting in mouse embryo-derived stem cells. *Cell* **51**, 503-512.

Thomas, K. R., Deng, C. and Capecchi, M. R. (1992). High-fidelity gene targeting in embryonic stem cells by using sequence replacement vectors. *Mol. Cell. Biol.* **12**, 2919-2923.

Wall, N. A., Jones, C. M., Hogan, B. L. M. and Wright, C. V. E. (1992). Expression and modification of *hox-2.1* protein in mouse embryos. *Mech. Dev.* **37**, 111-120.

Wilkinson, D. G., Bhatt, S., Chavrier, P., Bravo, R. and Charnay, P. (1989a). Segment-specific expression of a zinc-finger gene in the developing nervous system of the mouse. *Nature* **337**, 461-464.

Wilkinson, D. G., Bhatt, S., Cook, M., Boncinelli, E. and Krumlauf, R. (1989b). Segmental expression of *Hox-2* homeobox-containing genes in the developing mouse hindbrain. *Nature* **341**, 405-409.

Yokouchi, Y., Sasaki, H. and Kuroiwa, A. (1991). Homeobox gene expression correlated with the bifurcation process of limb cartilage development. *Nature* **353**, 443-445.

Yokouchi, Y., Nakazato, S., Yamamoto, M., Goto, Y., Kameda, T., Iba, H. and Kuroiwa, A. (1995). Misexpression of *Hoxa-13* induces cartilage homeotic transformation and changes cell adhesiveness in chick limb buds. *Genes Dev.* **9**, 2509-2522.

(Accepted 12 July 1996)